

# Rapid and Power-Aware Learned Optimization for Modular Receive Beamforming

Ohad Levy and Nir Shlezinger

**Abstract**—Multiple-input multiple-output (MIMO) systems play a key role in wireless communication technologies. A widely considered approach to realize scalable MIMO systems involves architectures comprised of multiple separate modules, each with its own beamforming capability. Such models accommodate cell-free massive MIMO and partially connected hybrid MIMO architectures. A core issue with the implementation of modular MIMO arises from the need to rapidly set the beampatterns of the modules, while maintaining their power efficiency. This leads to challenging constrained optimization that should be repeatedly solved on each coherence duration. In this work, we propose a power-oriented optimization algorithm for beamforming in uplink modular hybrid MIMO systems, which learns from data to operate rapidly. We derive our learned optimizer by tackling the rate maximization objective using projected gradient ascent steps with momentum. We then leverage data to tune the hyperparameters of the optimizer, allowing it to operate reliably in a fixed and small number of iterations while completely preserving its interpretable operation. We show how power efficient beamforming can be encouraged by the learned optimizer, via boosting architectures with low-resolution phase shifts and with deactivated analog components. Numerical results show that our learn-to-optimize method notably reduces the number of iterations and computation latency required to reliably tune modular MIMO receivers, and that it allows obtaining desirable balances between power efficient designs and throughput.

## I. INTRODUCTION

Massive multiple-input multiple-output (MIMO) technology is at the core of future wireless communications, with extremely large implementations expected to enable meeting the constantly growing demands in throughput and coverage [2], [3]. However, implementing communications with hundreds or thousands of antenna elements gives rise to several challenges, including issues related to cost, power consumption, deployment, and scalability [4]. To overcome these challenges, a leading approach to massive MIMO adopts *modular designs*. In such cases, an extremely large MIMO array is implemented using many distinct modules, each equipped with a (smaller) antenna array, and possibly possesses local beamforming capabilities. These modular architectures can take different forms, e.g., distributed cell-free massive MIMO [5], centralized interconnections of multiple panels [6], or radio stripes [7].

While modular implementations of massive MIMO alleviate cost and power issues and support distributed implementation, they also introduce design and algorithmic challenges. In particular, beamforming is not carried out by a single central

processing unit (CPU) that manipulates the signal at each element; instead, it is divided between the CPU and a set of separate arrays termed *panels*, that are possibly constrained in their hardware capabilities, and are likely to be subject to strict power constraints. Moreover, the setting of the modular beampattern is done on each coherence duration, necessitating rapid adjustments of the modules [8].

Since modular beamforming is divided between a CPU and multiple panels, it can be viewed as a form of *hybrid beamforming* [9]. Hybrid beamforming divides the processing of the signals between conventional digital processing and an additional constraint antenna interface, typically representing analog hardware [10]. Such hybrid MIMO is often studied in the context of RF chain reduction [11], [12], most commonly assuming phase shifter based analog processing [13]. However, hybrid MIMO can also represent emerging antenna architectures based on true-time-delay [14], vector modulators [15], metasurfaces [16], or leaky waveguides [17].

The main task of hybrid beamforming can be viewed as the conversion of channel state information (CSI) into a beampattern achievable through a divisible architecture [18]. Various methods have been proposed for tackling this task (see, e.g., overview in [19]). As hybrid beamforming can be represented as a constrained optimization problem, a conventional approach achieves this via iterative optimizers, see, e.g., [20]–[23]. However, these approaches typically involve lengthy optimization with numerous iterations, which can be challenging to carry out efficiently within the extremely short time frames required for determining beamforming (e.g., on the order of 0.1 milliseconds [19]).

To facilitate rapid beamforming setting, recent works proposed using deep learning tools, taking advantage of their ability to learn to tackle challenging optimization problems with fixed and limited latency [24], [25]. This can be achieved by training conventional deep learning architectures, such as convolutional neural networks (CNNs), to map MIMO CSI into analog and digital precoders [26], [27], or by combining optimization with deep learning for hybrid beamformers [28]–[32] as a form of model-based deep learning [33]. However, while hybrid beamforming can be viewed as encompassing modular beamforming, its associated algorithms are not tailored for exploiting modular structures, and do not account for the limited power considerations imposed in such forms of distributed MIMO systems. Moreover, current learning-aided designs often focus on a given configuration, and the optimizer needs to be retrained when using a different array (or adding another module), limiting scalability. Finally, existing works typically focus on downlink beamforming, with the uplink

Parts of this work were presented in the 2024 IEEE International Conference on Acoustics, Speech, and Signal Processing (ICASSP) as the paper [1]. This work was supported by the Israeli Innovation Authority. The authors are with the School of ECE, Ben-Gurion University of the Negev, Israel (e-mail: levyoha@post.bgu.ac.il; nirshl@bgu.ac.il).

being much less studied.

Uplink modular beamforming was considered in [34], [35]. There, the focus was to characterize trade-offs of its decentralization under narrowband communications and sparsity-based power-oriented constraints for loss-less processing, rather than establishing algorithms for tuning modular beamformers. In practice, the regimes of interest are typically those where the distributed and power constrained operation is likely to yield some rate loss compared to centralized fully digital MIMO systems. This gives rise to the need to design methods for tuning hybrid modular receive beamformers for such practical and challenging settings.

In this work, we develop a rapid and power-aware tuning algorithm for setting modular receive MIMO beamformers. Our approach combines principled optimization with machine learning via model-based deep learning [36] to realize uplink modular beamforming optimizers operating reliably with fixed and low latency. By doing so, we are able to utilize data to optimize the optimizer while maintaining its comprehensibility and transferability across different configurations.

We focus on modular beamformers implemented using conventional phase shifters, and leverage the interpretable operation of the optimizer to (i) facilitate scalable design, where the same learned optimizer can be utilized with different numbers of modules; and (ii) encourage power efficient designs for each panel. The latter is achieved by enabling deactivation and low-resolution implementation of the active phase shifters at each module. We formulate the modular uplink beamforming task as a constrained maximization of the sum-rate objective in multiple-access channels. We then specialize projected gradient ascent (PGA) steps with momentum for the considered setting, being a suitable candidate accelerated iterative optimizer for directly optimizing the rate objective, based on which we develop our learning-aided optimizer.

Our main contributions are summarized as follows:

- **First-order optimization for modular receive beamforming:** We formulate the receive modular beamforming task as a constrained optimization, and derive the corresponding first-order iterative optimizer based on PGA steps. We specifically characterize the corresponding gradient steps and projection methods, which enable (lengthy) tuning of modular receive beamformers.
- **Rapid and scalable learned optimization:** To enable rapid tuning, we convert the identified PGA steps into a machine learning model operating with a fixed and low latency. This is achieved by fixing the number of iterations while using the hyperparameters of PGA with momentum as trainable machine learning parameters. We show that the interpretable operation of the resulting design allows it to be applied to different number of modules (which can be much larger than those used in training), thus facilitating scalability.
- **Power-aware learned optimization:** We leverage the fact that the resulting machine learning model is comprised of interpretable PGA iterations to incorporate two forms of power-aware considerations: the ability to boost sparse modular architectures with deactivated phase shifters, and the support of low-resolution phase

shifters. As the resulting constraints render PGA non-differentiable, we approximate its operation for learning purposes via surrogate projection mappings that enable its representation as a machine learning architecture.

- **Extensive experimentation:** We extensively evaluate our learned optimizer for both synthetic channels as well as channels obtained from the physically compliant Quasi-Deterministic Radio channel Generator (QuaDRiGa) model [37]. Our numerical studies systematically show that learned optimization enables reliable tuning of modular beamformers with reductions of 10 – 30× in iterations compared to conventional optimizers, and that the power-aware design enables efficient operation with only a minor degradation in the accuracy compared to unconstrained designs.

The rest of this paper is organized as follows: Section II presents the system model of uplink modular beamforming and formulates its design problem. Section III presents our learned optimization method without accounting for power considerations, which are introduced into the method in Section IV. Empirical results are reported in Section V, and Section VI concludes the paper.

Throughout this paper, we use boldface lowercase and boldface uppercase letters for column vectors and matrices, respectively, while  $[\mathbf{M}]_{i,j}$  is the  $(i, j)$ th element of a matrix  $\mathbf{M}$ . We use calligraphic fonts for sets, while  $\mathbb{Z}$  and  $\mathbb{C}$  denote the integer and complex numbers, respectively. The operations  $(\cdot)^T$  and  $(\cdot)^H$  are used for transpose and conjugate transpose, respectively.  $\mathbf{I}_N$  refers to the identity matrix of size  $N$ . The gradient of the function  $f(\cdot)$  with respect to the matrix  $\mathbf{W}$  is denoted by  $\nabla_{\mathbf{W}} f(\cdot)$ , while  $\delta_{\cdot, \cdot}$  is the Kronecker delta function, and  $\angle(\cdot)$  is the (element-wise) phase operator (in radians).

## II. SYSTEM MODEL

In this section we introduce the system model for receive beamforming with modular hybrid MIMO receivers. We commence with presenting the considered models for the communication channel and the receiver processing in Subsections II-A-II-B, respectively, after which we formulate the beamforming design problem in Subsection II-C.

### A. Communication System

We consider a multi-band multi-user uplink MIMO system. The setting involves  $K$  single antenna users that communicate with a (possibly distributed) MIMO receiver, over  $B$  frequency bins. The transmitted signals are received by  $M$  antenna elements, that are divided into multiple panels. The channel output at the  $b$ th frequency is given by

$$\mathbf{y}[b] = \mathbf{H}[b]\mathbf{s}[b] + \mathbf{w}[b], \quad b = 1, \dots, B. \quad (1)$$

In (1),  $\mathbf{H}[b] \in \mathbb{C}^{M \times K}$  is the channel matrix at frequency bin  $b$ , while  $\mathbf{s}[b] \in \mathbb{C}^K$  represents the transmitted symbols, which are comprised of i.i.d. entries with power  $\rho_s > 0$ . The signal  $\mathbf{w}[b] \in \mathbb{C}^M$  is additive white Gaussian noise (AWGN) with variance  $\sigma_w^2 > 0$ .

## B. Modular Hybrid Receive Processing

The signal received by the  $M$  antenna elements is processed by a centralized CPU. The resulting digitally processed signal is obtained from the channel output in (1) by undergoing *modular receive beamforming*, where the  $M$  antennas are divided into  $P$  panels. This processing, illustrated in Fig. 1, includes two stages: (i) Panel-wise beamforming, and (ii) Panel-CPU connectivity.

1) *Panel-Wise Beamforming*: The first stage is composed of receive beamforming performed by each panel separately. Each panel has  $N$  antennas and  $L$  output ports, where the data processing takes place within the  $p$ th antenna panel and is described via a  $N \times L$  frequency-invariant matrix  $\mathbf{W}_p$ , for each  $p = 1, \dots, P$ . The panels are assumed to be hardware limited, which we model using the set of feasible mappings  $\mathcal{W} \subset \mathbb{C}^{N \times L}$ , such that  $\mathbf{W}_p \in \mathcal{W}$ .

We consider the following types of analog constraints:

C1 *Unconstrained Phase Shifters*: Here, the analog processing is comprised of phase shifters, where the phase of component can be set arbitrarily, i.e.,

$$\mathcal{W}_{\text{uph}} = \{ \mathbf{W} \in \mathbb{C}^{N \times L} : |[\mathbf{W}]_{n,l}| = 1, \forall(n,l) \}. \quad (2)$$

C2 *Sparsified Phase Shifters*: As phase shifters are active components with non-negligible power consumption, a candidate approach to maintain power-efficient operation at the panels is to allow some of the phase shifters to be turned off [15]. This type of feasible set is represented as

$$\mathcal{W}_{\text{sph}} = \{ \mathbf{W} \in \mathbb{C}^{N \times L} : |[\mathbf{W}]_{n,l}| \in \{0, 1\}, \forall(n,l) \}. \quad (3)$$

While the formulation in (3) does not indicate how many phase shifters are inactive, such a requirement can be imposed by constraining the  $\ell_0$  norm of  $\mathbf{W}$  to achieve a desired amount of inactive components.

C3 *Quantized Phase Shifters*: An alternative approach to limit the power consumption on the panel side is to restrict the phase shifters to support only a discrete set of feasible phases, i.e., support quantized phases shifts [38]. Such a constraint with  $Q$ -level quantized phases is modeled by the feasible set

$$\mathcal{W}_{\text{qps}}^Q = \{ \mathbf{W} \in \mathbb{C}^{N \times L} : \frac{\angle[\mathbf{W}]_{n,l}}{2\pi} \cdot Q \in \mathbb{Z}, \\ |[\mathbf{W}]_{n,l}| = 1, \forall(n,l) \}. \quad (4)$$

Note that for all considered feasible sets, the phase shifting components remain frequency-agnostic, i.e.,  $\mathbf{W}_p$  is invariant of the frequency index  $b$ . Moreover, we note that approaches C2 and C3, which aim to improve the power efficiency of the panels, are complementary. Accordingly, one can restrict the analog processing at the panels side to be both sparse and quantized, i.e., have some of the phase shifters deactivated, while the active ones take discrete phase values.

2) *Panel-CPU Connectivity*: We model the connectivity to the CPU via the binary matrix  $\mathbf{A} \in \{0, 1\}^{L \cdot P \times T}$ , with  $T$  being the number of CPU inputs. This matrix is also frequency invariant, and its entry  $[\mathbf{A}]_{l \cdot p, t}$  denotes whether the  $l$ th output of the  $p$ th panel is connected to the  $t$ th CPU input. The CPU input  $z[b]$  is related to the channel output  $\mathbf{y}[b]$  via

$$z[b] = \mathbf{A}^H \mathbf{W}^H \mathbf{y}[b], \quad (5)$$

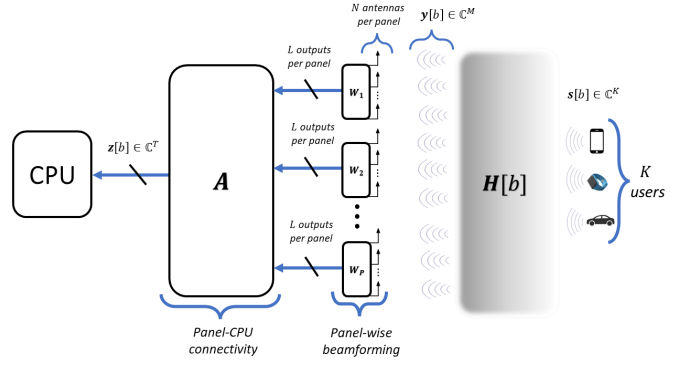


Fig. 1: Modular hybrid receive processing chain.

where  $\mathbf{W} = \text{blkdiag}\{\mathbf{W}_1, \dots, \mathbf{W}_P\}$ . This constraint comes from the decentralized structure of our communication system, which takes place within each panel. Note that when  $\mathbf{A}$  is the identity matrix and  $L = 1$ , this formulation specializes the common form of partially-connected hybrid beamformers [11].

## C. Problem Formulation

We aim to design the modular receive beamformer detailed in (5) to maximize the achievable rate. To formulate this, we define the equivalent channel at the  $b$ th frequency bin as  $\mathbf{G} \triangleq \mathbf{W}\mathbf{A} \in \mathbb{C}^{M \times T}$ . For the uplink setup detailed in Subsection II-A, the average achievable sum-rate is given by (see, e.g., [39, Thm. 1])

$$R(\mathbf{G}; \{\mathbf{H}[b]\}) = \frac{1}{B} \sum_{b=1}^B \log \left| \mathbf{I}_M + \frac{\rho_s}{N_0} \mathbf{G}(\mathbf{G}^H \mathbf{G})^{-1} \right. \\ \left. \mathbf{G}^H \mathbf{H}[b] \mathbf{H}^H[b] \right|. \quad (6)$$

Using the rate expression in (6), we can formulate the setup of modular receive beamforming as a constrained optimization problem. Since the matrix  $\mathbf{A}$  represents the hardware connectivity between the panels, it is assumed to be constant. Accordingly, for a given channel realization  $\{\mathbf{H}[b]\}_{b=1}^B$ , the modular beamforming task is formulated as the recovery of

$$\mathbf{W}^* = \arg \max_{\mathbf{W} = \text{blkdiag}\{\mathbf{W}_1, \dots, \mathbf{W}_P\}} R(\mathbf{W}\mathbf{A}; \{\mathbf{H}[b]\}) \quad (7) \\ \text{subject to } \mathbf{W}_p \in \mathcal{W}, \quad \forall p \in \{1, \dots, P\}.$$

The problem as it is formulated in (7) considers a generic setting for the feasible panel-wise computation set  $\mathcal{W}$ . As such, it accommodates both the unstructured setting C1 as well as the power-oriented C2-C3. However, when required to operate with sparse panels C2, one is likely to also impose an additional constraint on the overall number of active phase shifters in  $\mathbf{W}$ . Similarly, imposing C3 assumes that one operates with a fixed and known resolution dictated by  $Q$ .

In some cases (e.g., when  $T \geq \max(\lfloor M \frac{K-L}{K} + 1 \rfloor, K)$ ,  $B = 1$ , and while allowing  $\mathcal{W} = \mathbb{C}^{N \times L}$ ), one can identify the optimal setting [34]. Even in such cases, tackling (7) typically involves an iterative optimization procedures. In practice, the modular beamformer must be set within a coherence duration (which can be of the order of 0.1 milliseconds [19]). To account for this requirement, we limit the number of iterations

for these calculations, allowing at most  $J$  iterations. To facilitate identifying an optimizer that can reliably tackle (7) within  $J$  iterations, we assume access to a data set  $\mathcal{D}$  composed of  $|\mathcal{D}| > 0$  past channel realizations, i.e.,

$$\mathcal{D} = \left\{ \left\{ \mathbf{H}_i[b] \right\}_{b=1}^B \right\}_{i=1}^{|\mathcal{D}|}. \quad (8)$$

### III. UNCONSTRAINED UNFOLDED MODULAR BEAMFORMING

In this section, we study modular beamforming design while focusing on *unconstrained phase shifters*, i.e., constraint C1. The unfolded modular beamforming algorithm, which is geared towards enabling rapid adaptation, serves as a starting point for considering the more restrictive constraints C2-C3 in Section IV. In particular, we first formulate our baseline optimizer of PGA with momentum in Subsection III-A. Then, we convert it into a machine learning model in Subsection III-B, and provide a discussion in Subsection III-C.

#### A. PGA with Momentum

A direct approach to tackle (7) employs first-order methods [40], e.g., PGA. This scheme starts from some initial guess  $\mathbf{W}_0$ , and iteratively takes gradient steps towards the maximization of (6), projected to meet the constraints. PGA relies on the ability to compute the gradient of  $R(\mathbf{W}\mathbf{A}; \{\mathbf{H}[b]\})$  with respect to  $\mathbf{W}$ , denoted  $\nabla_{\mathbf{W}} R(\mathbf{W}, \mathbf{A})$ . The gradient of the rate is stated in Theorem 1.

*Theorem 1:* The gradient of (6) with respect to  $\mathbf{W}$  is

$$\begin{aligned} \nabla_{\mathbf{W}} R(\mathbf{W}, \mathbf{A}) &= \frac{1}{B} \sum_{b=1}^B \left( \frac{\rho_s}{\sigma_w^2} \mathbf{A} \left( (\mathbf{G}^H \mathbf{G})^{-1} \mathbf{G}^H \right. \right. \\ &\quad \times \mathbf{H}[b] \mathbf{H}[b]^H \left. \left. \left( \mathbf{I} + \frac{\rho_s}{\sigma_w^2} (\mathbf{G}^H \mathbf{G})^{-1} \mathbf{G}^H \right. \right. \right. \\ &\quad \left. \left. \left. \times \mathbf{H}[b] \mathbf{H}[b]^H \right) \right)^{-1} \left( \mathbf{I} - \mathbf{G} (\mathbf{G}^H \mathbf{G})^{-1} \mathbf{G}^H \right) \right)^H. \quad (9) \end{aligned}$$

*Proof:* The proof is given in Appendix A. ■

In addition to the gradient in (9), one should also be able to project onto the feasible constraints in (7) to formulate PGA. For the non-power-constrained feasible set (2), the projection operator for a matrix  $\mathbf{W}$  based on C1 is

$$[\mathcal{P}_{\mathcal{W}_{\text{uph}}}(\mathbf{W})]_{i,j} = \frac{[\mathbf{W}]_{i,j}}{||[\mathbf{W}]_{i,j}||} \cdot \delta_{\lfloor \frac{i}{N} \rfloor, \lfloor \frac{j}{L} \rfloor}. \quad (10)$$

In (10), the element-wise operation divides each entry of the matrix  $\mathbf{W}$  by its own magnitude, and then sets it to zero if it falls out of the main block diagonal. This effectively keeps each panel-wise processing made up of phase-shifters only.

Although first-order methods often require a large number of iterations to converge, they can typically be accelerated by introducing momentum. Momentum is also useful for dealing with non-convex objectives, as in (7), since it can prevent getting trapped in local minima and saddle points. The resulting PGA with momentum is summarized as Algorithm 1.

---

#### Algorithm 1: PGA with Momentum

---

**Init:** Initialize  $\mathbf{W}_{-1}$  as zeros; randomize  $\mathbf{W}_0$ .  
Set iterations  $J$ , hyperparameters  $\{\mu_j, \beta_j\}_{j=0}^{J-1}$ .  
**Input:**  $\{\mathbf{H}[b]\}_{b=1}^B, \mathbf{A}$   
**1 for**  $j = 0, 1, \dots, J - 1$  **do**  
**2**   Compute gradient  $\nabla_{\mathbf{W}} R(\mathbf{W}_j, \mathbf{A})$  via (9);  
**3**   Take gradient step  
     $\mathbf{W}_{j+1} \leftarrow \mathbf{W}_j + \mu_j \nabla_{\mathbf{W}} R(\mathbf{W}_j, \mathbf{A})$ ;  
**4**   Add momentum  
     $\mathbf{W}_{j+1} \leftarrow \mathbf{W}_{j+1} + \beta_j (\mathbf{W}_j - \mathbf{W}_{j-1})$ ;  
**5**   Project  $\mathbf{W}_{j+1} \leftarrow \mathcal{P}_{\mathcal{W}_{\text{uph}}}(\mathbf{W}_{j+1})$  via (10);  
**6 return**  $\mathbf{W}_J$

---

#### B. Unfolded PGA with Momentum

Algorithm 1 allows tackling (7) while meeting the requirement to operate with  $J$  iterations. However, iterative optimizers such as PGA are designed to tackle convex optimization problems and to operate with asymptotically large number of iterations. There, convergence can be guaranteed with fixed hyperparameters  $\{\mu, \beta\}$  (i.e., independent of the iteration index  $j$ ), which can be tuned manually. In Algorithm 1, we apply this convex optimizer to a non-convex problem (7) while operating with a fixed and small number of iterations  $J$ . In such cases, the setting of the hyperparameters  $\{\mu_j, \beta_j\}$  greatly affects performance [40, Ch. 9]. This motivates leveraging the available data in (8) to tune these hyperparameters, by converting Algorithm 1 into a discriminative machine learning model [41], and proposing a dedicated learning mechanism. We next detail the resulting machine learning architecture, its proposed training procedure, and how it can be scaled to large modular settings.

1) *Architecture:* Algorithm 1 operates with exactly  $J$  iterations. It can thus be readily converted into a machine learning model via deep unfolding for learning hyperparameters [33]. Here, each iteration is treated as a layer in a multi-layer architecture, whose trainable weights are the hyperparameters.

We increase the abstractness of the trainable architecture by allowing it to use different values of  $\mu$  and  $\beta$  not just per iteration, but also per entry in  $\mathbf{W}$ . Accordingly, the scalar values  $\{\mu_j, \beta_j\}$  that multiply matrix quantities in Algorithm 1 are replaced with block-diagonal matrices  $\alpha_j, \beta_j$  that multiply the matrix quantities in Algorithm 1 element-wise. The resulting architecture obtained from Algorithm 1 is illustrated in Fig. 2, and has  $2 \cdot J \cdot P \cdot N \cdot L$  trainable parameters, written as

$$\boldsymbol{\theta} = \{\alpha_j, \beta_j\}_{j=0}^{J-1}. \quad (11)$$

2) *Training:* Converting Algorithm 1 into a machine learning model facilitates tuning  $\boldsymbol{\theta}$  in (11), which are the hyperparameters of Algorithm 1. This is achieved using the dataset  $\mathcal{D}$  in (8), containing past channel realizations taken from the same communication system. Letting  $\mathbf{W}_J(\boldsymbol{\theta})$  be the modular beamforming matrix computed by Algorithm 1 with parameters  $\boldsymbol{\theta}$ , we seek the hyperparameters

$$\boldsymbol{\theta}^* = \arg \max_{\boldsymbol{\theta}} \sum_{\{\mathbf{H}[b]\} \in \mathcal{D}} R(\mathbf{W}_J(\boldsymbol{\theta}) \mathbf{A}; \{\mathbf{H}[b]\}). \quad (12)$$

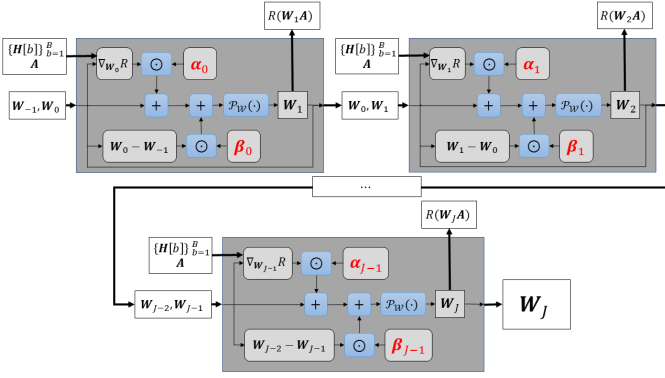


Fig. 2: Architecture, trainable parameters marked with red.

The objective in (12) evaluates  $\theta$  based on the output of the unfolded architecture, i.e.,  $\mathbf{W}_J$ . To facilitate the learning of  $\theta$ , we exploit the interpretability of the architecture, and particularly the fact that each layer should output a gradually improved modular beamformer. Accordingly, we propose a loss measure for optimizing  $\theta$  that accounts for the output of the intermediate iterations (layers) in a monotonically growing fashion. Specifically, we use a loss function with logarithmic contribution growth between iterations [42], [43], given by

$$\mathcal{L}_{\mathcal{D}}(\theta) = - \sum_{\{\mathbf{H}[b]\} \in \mathcal{D}} \sum_{j=1}^J \frac{\log(1+j)}{|\mathcal{D}|} R(\mathbf{W}_j(\theta)\mathbf{A}; \{\mathbf{H}[b]\}).$$

The resulting training algorithm using mini-batch stochastic gradient descent is stated as Algorithm 2. The negative sign in the loss is added because our objective is to maximize the rate, rather than minimize it.

---

#### Algorithm 2: Learning Hyperparameters

---

**Init:** Set  $\theta$  as fixed hyperparameters

Fix learning rate  $\eta > 0$  and epochs  $i_{\max}$

**Input:** Training set  $\mathcal{D}$

```

1 for  $i = 0, 1, \dots, i_{\max} - 1$  do
2   Randomly divide  $\mathcal{D}$  into  $Q$  batches  $\{\mathcal{D}_q\}_{q=1}^Q$ ;
3   for  $q = 1, \dots, Q$  do
4     Apply model with parameters  $\theta$  to  $\mathcal{D}_q$ ;
5     Update  $\theta \leftarrow \theta - \eta \nabla_{\theta} \mathcal{L}_{\mathcal{D}_q}(\theta)$ ;

```

6 return  $\theta$

---

3) *Transferability Across Configurations:* Modular beamforming architectures are scalable, stemming from the ability to achieve extremely large MIMO configurations by adding panels. A core gain of our interpretable learning-aided optimizers is the fact that they support such scalability. Specifically, what we learn are hyperparameters of an optimization algorithm, which can be applied to different configurations. This indicates that our unfolded optimizer shares this transferability across configurations, thus inherently supporting large and adaptive scale deployments.

In particular, the architecture and training procedure detailed above are formulated for a given modular configuration. Nonetheless, a learned optimizer is transferable, and a learned optimizer trained for a small configuration can be scaled to

applied to much larger ones. Specific scalable parameters of interest are the numbers of users  $K$  and of panels  $P$ :

- *Scaling  $K$ :* we note that the learned hyperparameters in (11) are invariant of the number of users. Thus, a learned optimizer trained for a small number of users can be readily applied to a setting with a large number of users.
- *Scaling  $P$ :* While the setting of the hyperparameters in (11) depends on the number of hyperparameters, as we allow panel-specific hyperparameters, one can scale by reusing hyperparameters across panels [44]. For instance, a learned optimizer trained to set  $\{\alpha_j, \beta_j\}$  for a configuration with  $P$  panels can be applied to a setting with  $c \cdot P$  a positive integer  $c$ , by e.g., setting its hyperparameters to be  $\{\mathbf{I}_c \otimes \alpha_j, \mathbf{I}_c \otimes \beta_j\}$ , where  $\otimes$  denotes the Kronecker product, or by assigning the added panels an average of the learned hyperparameters.

The above approaches to transfer a learned optimizer across different configurations are empirically demonstrated to yield effective and scalable optimization in Subsection V-B2.

#### C. Discussion

The proposed unfolded PGA is designed to learn from data how to traverse the optimization loss surface, allowing to achieve improved sum-rate within  $J$  iterations, as shown in Section V. The resulting learned  $\theta$ , which represents the per-iteration hyperparameters used for setting the modular beamformer, may exhibit certain counter-intuitive characteristics, such as negative gradient steps, as means of coping with non-convexity. As the resulting algorithm is a learned implementation of a principled optimizer, we share its scalability, which is highly desirable in modular architectures. While our formulation considers panels comprised phase-shifters, one can consider alternative hardware, such as distributed active metasurfaces [39] and phase-time arrays [45].

The fixed and limited number of iterations impacts the computational complexity of setting the modular beamformers for a given channel realization. To quantify this complexity, we examine a single iteration of Algorithm 1. The computational burden is mainly dominated by the *gradient computation* step, formulated in (9). This computation has a complexity order (in complex multiplications) of

$$\mathcal{O}\left(B(T^3 + M^2(T + K)) + M(T^2 + LPT + TK)\right). \quad (13)$$

The remaining steps in the algorithm include the *update step* and the *projection step* (10). The complexity order of these steps is  $\mathcal{O}(MLP)$  for both, which is negligible compared to the gradient computation step. Considering that optimization procedure operates over  $B$  frequency bins, the overall complexity of the PGA+M algorithm with a predefined  $J$  iterations, as implemented by the proposed learned optimizer, is of the order of

$$\mathcal{C}_{PGA+M} = \mathcal{O}\left(JB\left(T^3 + M^2(T + K) + M(T^2 + LPT + TK)\right)\right). \quad (14)$$

The asymptotic complexity characterization in (14) is comprised of multiple summands, where in general none of the terms can be consistently ignored. Nonetheless, in an expected massive modular MIMO setting, where the overall number of antenna elements is larger than both the number of users ( $K$ ) and the number of CPU inputs ( $T$ ), the dominating term is the one growing quadratically with  $M$ , and thus  $\mathcal{C}_{PGA+M} \approx \mathcal{O}(JBTM^2)$ . When delving further into the analysis, it becomes evident that the dominant terms (in complex products) arise from matrix multiplication operations. However, these computations can often be parallelized to reduce computational complexity, making the complexity of matrix inversion, represented by the  $\mathcal{O}(JBT^3)$  term, the dominant factor. While it is possible to further reduce the number of multiplication operations through techniques such as sparse and low-rank approximations of the gradients, we leave this aspect to future research.

#### IV. POWER-AWARE UNFOLDED MODULAR BEAMFORMING

Our analysis in Section III focused on the unconstrained setting C1. In this section, we use the unconstrained design for maximizing the rate (6) as a starting point, on top of which we develop a power-aware design. Specifically, we leverage the interpretability of the solution described in Section III to incorporate constraints C2-C3. We focus on conventional (non-learned) gradient-based optimization subject to C2-C3 in Subsections IV-A and IV-B, respectively. Then, we formulate PGA with momentum and the unfolded algorithms tailored for these designs in Subsections IV-C and IV-D, respectively, and conclude with a discussion in Subsection IV-E.

##### A. Sparsified Modular Beamformer

As detailed in Section II, power efficiency can be enhanced by turning off some of the phase shifters. Supporting deactivated phase shifters can be mathematically accommodated by constraint C2, i.e., as promoting sparsity of the matrix  $\mathbf{W}$ . To meet this constraint, we rewrite our constrained optimization from (7) as

$$\begin{aligned} \mathbf{W}^* = & \arg \max_{\mathbf{W}=\text{blkdiag}\{\mathbf{W}_1, \dots, \mathbf{W}_P\}} R(\mathbf{W}\mathbf{A}; \{\mathbf{H}[b]\}) \quad (15) \\ & \text{subject to } \|\mathbf{W}\|_0 \leq S_{\max} \\ & \mathbf{W}_p \in \mathcal{W}_{\text{sph}}, \quad \forall p \in \{1, \dots, P\}, \end{aligned}$$

where  $S_{\max} \leq N \cdot L \cdot P$  represents the maximal allowed number of active phase shifters. In (15), each phase shifter can be either active or turned off (by (3)). The  $\ell_0$  constraint guarantees that at most  $S_{\max}$  phase shifters are active.

Due to the inherent challenges associated with gradient-based optimization under  $\ell_0$  constraints, we adopt the common approach of relaxing it into an  $\ell_1$  constraint (see, e.g., [46, Ch. 1]). The relaxed optimization problem is

$$\begin{aligned} \mathbf{W}^* = & \arg \max_{\mathbf{W}=\text{blkdiag}\{\mathbf{W}_1, \dots, \mathbf{W}_P\}} R(\mathbf{W}\mathbf{A}; \{\mathbf{H}[b]\}) - \lambda \|\mathbf{W}\|_1 \\ & \text{subject to } \mathbf{W}_p \in \mathcal{W}_{\text{sph}}, \quad \forall p \in \{1, \dots, P\}. \end{aligned} \quad (16)$$

In (16),  $\lambda > 0$  is an objective regularization coefficient [33] whose purpose is to encourage the solution to hold the sparsity constraint in (15). Setting the exact value of such hyperparameters to meet a desired sparsity level  $S_{\max}$  is typically elusive, and involves repeating numerical trials to identify the exact value that strikes a desired trade-off between performance (i.e., rate) and sparsity. Nonetheless, once  $\lambda$  is fixed, the gradient of the relaxed objective in (16) can be computed as

$$\begin{aligned} \nabla_{\mathbf{W}} \left( R(\mathbf{W}\mathbf{A}; \{\mathbf{H}[b]\}) - \lambda \|\mathbf{W}\|_1 \right) = \\ \nabla_{\mathbf{W}} R(\mathbf{W}\mathbf{A}; \{\mathbf{H}[b]\}) - \lambda \cdot e^{j\angle \mathbf{W}}. \end{aligned} \quad (17)$$

where  $\nabla_{\mathbf{W}} R(\cdot)$  is given in Theorem 1.

Relaxing (15) into (16) enables computing the objective gradients via (17). In order to enable PGA-based optimization, one should also define the corresponding projection on the feasible set  $\mathcal{W}_{\text{sph}}$ . To that end, we adopt a flexible extension of the projection operator in (10) to account for deactivated phase shifters, by introducing a magnitude threshold  $\zeta > 0$ . The resulting projection step is given by

$$[\mathcal{P}_{\mathcal{W}_{\text{sph}}}(\mathbf{W})]_{i,j} = \begin{cases} \frac{[\mathbf{W}]_{i,j}}{\|[\mathbf{W}]_{i,j}\|} \cdot \delta_{\lfloor \frac{i}{N} \rfloor, \lfloor \frac{j}{L} \rfloor} & |[\mathbf{W}]_{i,j}| \geq \zeta, \\ 0 & |[\mathbf{W}]_{i,j}| < \zeta. \end{cases} \quad (18)$$

Projection via (18) is a crucial step in the tackling the relaxation of (15), ensuring that we set some elements of  $\mathbf{W}$  to 0 and constrain their magnitude to be either 0 or 1, as described in C2. At the same time, this step preserves the block diagonal structure of  $\mathbf{W}$ . A candidate choice of  $\zeta$  is  $\zeta = 0.5$ ; Setting  $\zeta = 0$  makes this projection step coincide with the projection step in (10).

##### B. Quantized Modular Beamformer

A complementary approach to mitigate power consumption of analog modular processing is by discretizing the phase resolution with a few bit representation. Incorporating the resulting constraint C3 into the rate maximization objective (7), yields the resulting constrained optimization formulation

$$\begin{aligned} \mathbf{W}^* = & \arg \max_{\mathbf{W}=\text{blkdiag}\{\mathbf{W}_1, \dots, \mathbf{W}_P\}} R(\mathbf{W}\mathbf{A}; \{\mathbf{H}[b]\}) \quad (19) \\ & \text{subject to } \mathbf{W}_p \in \mathcal{W}_{\text{qps}}^Q, \quad \forall p \in \{1, \dots, P\}. \end{aligned}$$

In (19), the set of feasible phase shifts is restricted to take  $Q$  quantization levels, using the definition of  $\mathcal{W}_{\text{qps}}^Q$  in (4).

We note that the objective in (19) is the same as in the unconstrained case (7), and thus its gradient can be obtained from Theorem 1. Consequently, to formulate the suitable PGA steps for tackling (19), one must specify the quantization-aware projection operator. A direct approach to guarantee discrete phase components is by setting each phase element into its nearest discrete value, resulting in

$$\begin{aligned} [\mathcal{P}_{\mathcal{W}_{\text{qps}}^Q}(\mathbf{W})]_{i,j} = & e^{j\phi_{i,j}^*} \cdot \delta_{\lfloor \frac{i}{N} \rfloor, \lfloor \frac{j}{L} \rfloor} \quad (20) \\ & \text{where } \phi_{i,j}^* = \arg \min_{\frac{\phi}{2\pi} \in \mathbb{Z}} |\phi - \angle[\mathbf{W}]_{i,j}|. \end{aligned}$$

The projection operator in (20) can be viewed as uniform scalar quantization of the phase of each element of  $\mathbf{W}$ .

### C. Power Aware PGA

Here we present a baseline PGA algorithm for the updated set of constraints, as described in C2 and C3. This PGA algorithm is an extension of Algorithm 1, adapted to the power aware objectives described in Subsections IV-A and IV-B. The resulting formulation is summarized as Algorithm 3. There, we integrate the power-aware gradient formulation (17) with the projection steps (18) and (20) to realize PGA.

---

#### Algorithm 3: Power-Aware PGA with Momentum

---

**Init:** Initialize  $\mathbf{W}_{-1}$  as zeros; randomize  $\mathbf{W}_0$ ;  
 Choose projection operator  $\mathcal{P}_{\mathcal{W}}(\cdot)$ ;  
 Set iterations  $J$ , hyperparameters  $\{\mu_j, \beta_j\}_{j=0}^{J-1}, \lambda$ ;  
**Input:**  $\{\mathbf{H}[b]\}_{b=1}^B, \mathbf{A}$   
 1 **for**  $j = 0, 1, \dots, J - 1$  **do**  
 2     Set gradient  $\nabla_{\mathbf{W}}(R(\mathbf{W}_j \mathbf{A}) - \lambda \|\mathbf{W}\|_1)$  via (17);  
 3     Take gradient step  
        $\mathbf{W}_{j+1} \leftarrow \mathbf{W}_j + \mu_j \nabla_{\mathbf{W}}(R(\mathbf{W}_j \mathbf{A}) - \lambda \|\mathbf{W}\|_1)$ ;  
 4     Add momentum  
        $\mathbf{W}_{j+1} \leftarrow \mathbf{W}_{j+1} + \beta_j (\mathbf{W}_j - \mathbf{W}_{j-1})$ ;  
 5     Project  $\mathbf{W}_{j+1} \leftarrow \mathcal{P}_{\mathcal{W}}(\mathbf{W}_{j+1})$  via (18) or (20);  
 6 **return**  $\mathbf{W}_J$

---

Algorithm 3 is designed to tackle the maximization problems outlined in (16) and (19) by proper settings of the projection operator and the regularization coefficient. For instance, by setting the projection to be given in (20) and setting  $\lambda = 0$ , Algorithm 3 tackles problem (19). Similarly, by using  $\lambda > 0$  and setting the projection to be (18), it tackles problem (16).

### D. Unfolded Power Aware PGA

In Subsection III-B, we showed how data can be leveraged to tune the hyperparameters of Algorithm 1 to enhance its performance within  $J$  iterations, by converting it into a machine learning architecture. Here, we follow this methodology to convert the power-aware Algorithm 3 into a trainable architecture. As opposed to the unconstrained case, where the learned hyperparameters were solely associated with the solver, i.e., with PGA, in the following we also leverage data to tune parameters associated with the optimization objective [33], and particularly the (typically elusive) regularization coefficient  $\lambda$ .

1) *Architecture:* Following the conversion of PGA with momentum into a machine learning model in Subsection III-B1, we view the iterative algorithm as a multi-layer architecture. This allows using the data (8) to learn hyperparameters that yield desirable settings within a few iterations.

Algorithm 3 introduces another hyperparameter,  $\lambda$ , associated with optimization objective, and particularly the  $\ell_1$  norm reduction. Here, we increase the abstractness of the trainable architecture by allowing  $\lambda$  to differ from one iteration to another, i.e., have each iteration taking its gradient step over a *different loss surface*. Furthermore, we turn the scalar regularization coefficient into a matrix with different values for each entry in  $\mathbf{W}$ . We add these learnable matrices  $\{\boldsymbol{\lambda}_j\}_{j=0}^{J-1}$  to

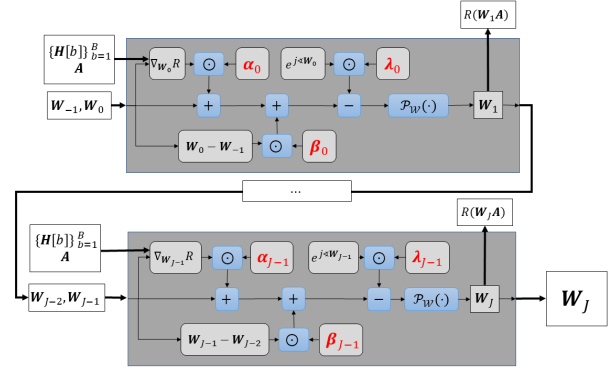


Fig. 3: Power aware unfolded architecture, trainable parameters marked with red.

the set of trainable parameters  $\theta$ . Accordingly, we now have  $3 \cdot J \cdot P \cdot N \cdot L$  trainable parameters, written as

$$\theta = \{\alpha_j, \beta_j, \lambda_j\}_{j=0}^{J-1}. \quad (21)$$

The power aware architecture is visualized in Fig. 3 for a given learned hyperparameters  $\theta$ . For clarity of presentation, in Fig. 3 we separate the gradient step in Algorithm 3 into two separate steps, each one dependent on a different hyperparameter.

2) *Projection:* A key issue in deep unfolding is maintaining the forward path differentiable. This allows the optimizer to be represented as a trainable architecture that can be tuned with deep learning techniques based on backpropagation [33]. Algorithm 3 mainly differs from Algorithm 1 in the projection step. The projection step in both (18) and (20) contains continuous-to-discrete mappings that nullify gradients.

To overcome this, we distinguish between the projection step utilized when applying the optimizer, and a differentiable surrogate utilized for evaluating gradients during training. Specifically, we use the following surrogate projections:

- *Approximating  $\mathcal{P}_{\mathcal{W}_{\text{sph}}}$ :* The projection onto  $\mathcal{W}_{\text{sph}}$  can be viewed as a step function. Accordingly, we approximate it during training using a harp and shifted sigmoid function [47] denoted  $\hat{\mathcal{P}}_{\mathcal{W}_{\text{sph}}}$ , given by

$$[\hat{\mathcal{P}}_{\mathcal{W}_{\text{sph}}}]_{i,j} = |\mathbf{W}_{i,j}| = \sigma(s_m(|\mathbf{W}_{i,j}| - \zeta_m)). \quad (22)$$

In (22)  $\sigma$  denoting the sigmoid function,  $s_m$  denotes a sharpness hyperparameter, and  $\zeta_m$  stands for the shift, imitating the threshold  $\zeta$  from (18).

- *Approximating  $\mathcal{P}_{\mathcal{W}_{\text{qph}}}$ :* For phase approximation with  $Q$  quantization levels, we note that the projection operator is a piecewise-constant monotonically increasing function. Following [48], we approximate the quantization levels with sum of  $Q$  differently shifted sigmoid functions. The resulting phase projection sets  $\phi_{i,k}^*$  in (20) to be

$$\hat{\phi}_{i,k}^* = \frac{2\pi}{Q} \sum_{q=1}^Q \sigma\left(s_p\left(\angle \mathbf{W}_{i,j} - \frac{2\pi(q-0.5)}{Q} + \pi\right)\right), \quad (23)$$

where  $s_p$  is a sharpness hyperparameter.

This above formulations approximate the projection operators in a differentiable manner, ensuring smooth gradients

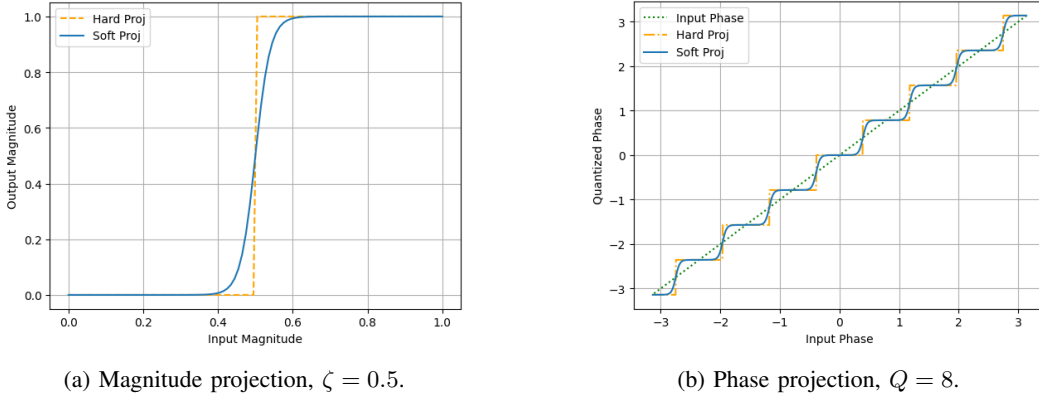


Fig. 4: Projection operators for power-aware PGA and their corresponding differentiable approximation.

during training while maintaining the characteristics of the original projection step. The ability of (20)-(23) to approximate their corresponding hard (non-differentiable) projection operators is illustrated in Fig. 4.

3) *Loss Function*: We assume access to a dataset  $\mathcal{D}$ , which comprises past channel realizations. This data is leveraged to learn the hyperparameters for solving the following constrained optimization problem:

$$\theta^* = \arg \max_{\theta} \sum_{\{\mathbf{H}[b]\} \in \mathcal{D}} R(\mathbf{W}_J(\theta)\mathbf{A}; \{\mathbf{H}[b]\}) \quad (24)$$

subject to:  $\mathbf{W}_J = \text{blkdiag}\{\mathbf{W}_{J_1}, \dots, \mathbf{W}_{J_P}\}$

(i)  $\|\mathbf{W}_{J_p}\|_0 \leq S_{\max}$ ,  $\mathbf{W}_{J_p} \in \mathcal{W}_{\text{sph}}$ ,  $\forall p \in \{1, \dots, P\}$ .

(ii)  $\mathbf{W}_{J_p} \in \mathcal{W}_{\text{qps}}$ ,  $\forall p \in \{1, \dots, P\}$ .

The constraints on  $\mathbf{W}$  are either (i) or (ii), depending on the solved problem, (15) or in (19), respectively.

The learning objective in (24) under (i) encapsulates a key difference from the unconstrained one (12). Specifically, for sparse phase shifters, the learning objective stems from (15), namely, maximizing  $R$  under the  $\ell_0$  norm constraint. When formulating the resulting PGA iterations, we relaxed  $\ell_0$  norm to the  $\ell_1$  norm, using the coefficient  $\lambda$  to balance between rate maximization ( $R$ ) and sparsification. To translate this into a suitable loss for training that encourages a desired  $\ell_1$  norm, we introduce the following training loss

$$\mathcal{L}_{\mathcal{D}}(\theta) = -\frac{1}{|\mathcal{D}|} \sum_{\{\mathbf{H}[b]\} \in \mathcal{D}} \sum_{j=1}^J \log(1+j) R(\mathbf{W}_j(\theta)\mathbf{A}; \{\mathbf{H}[b]\}) - \gamma (\|\mathbf{W}_J(\theta)\|_1 - S_{\max})^2, \quad (25)$$

where  $\gamma \geq 0$  is a regularization hyperparameter. The loss (25) is also used with quantized phase shifters, i.e., under (ii), by setting  $\gamma = 0$ , as constraint (ii) is guaranteed to hold when using the projection operator  $\mathcal{P}_{\mathcal{W}_{\text{qps}}}$  in modular beamforming.

The updated loss function (25) is an extension of the unconstrained loss function (12), adding the squared error between the  $\ell_1$  norm of  $\mathbf{W}_J$  and  $S_{\max}$ . The rationale stems from our desire to encourage  $\|\mathbf{W}_J\|_1$  (being a differentiable approximation of  $\|\mathbf{W}_J\|_0$ ) to approach  $S_{\max}$  without having to tune different regularization coefficients for different  $S_{\max}$ . This allows training via, e.g., mini-batch stochastic gradient descent, as in Algorithm 2.

### E. Discussion

The design of the constrained modular beamformer via Algorithm 3 is based on the PGA steps designed for the unconstrained setting in Algorithm 1, leveraging its interpretable operation by introducing dedicated projections. Despite the similarity in inference, the procedure involved in learning the hyperparameters from data substantially differs from the unconstrained case, necessitating differentiable approximations of the projection operators during learning, altering gradient computation, and a dedicated training loss. This allows learning to rapidly set constrained modular beamformers with only a minor degradation in the rate, as shown in Section V.

Once the hyperparameters are learned through the unfolded learning procedure detailed in Subsection IV-D, the setting of the modular beamformer in Algorithm 3 follows the unconstrained PGA in Algorithm 1. The key differences are the additional phase term in the gradient computations via (17), and the modification of the projection operators via (18) or (20). As none of these operations dominates the computational burden, the complexity of the power-aware design is similar to that of the unconstrained case, analyzed in Subsection III-C.

Our power-aware design boosts power efficiency by supporting deactivated and low-resolution phase shifters. The translation of these properties into power savings is highly dependent on the hardware. We opt for a parametric representation of the desired sparsity level and phase shifter resolution, allowing the unfolded optimizer to be useful for different implementations and different power levels by setting of the corresponding parameters, e.g.,  $S_{\max}$  and  $Q$ . While our learning procedure utilizes the projection surrogates visualized in Fig. 4, one can consider alternative differentiable approximations of such continuous-to-discrete mappings, see, e.g., [49]. Moreover, additional methods to boost power efficiency by, e.g., deactivating panels rather than phase shifters, can be obtained as extensions to our framework, which are left for future study.

## V. EXPERIMENTAL STUDY

In this section, we numerically evaluate the proposed unfolded algorithm for rapid tuning of uplink modular beamforming<sup>1</sup>. We describe the experimental setup in Subsec-

<sup>1</sup>The source code and hyperparameters are available at <https://github.com/levyohad/Power-Aware-Deep-Unfolding-for-Beamforming>



tion **V-A**, while our results for unconstrained and power-aware settings are reported in Subsections **V-B-V-C**, respectively.

### A. Experimental Setup

We simulate a communication system, where the channel matrices  $\{\mathbf{H}[b]\}_{b=1}^B$  are obtained from a Rayleigh fading distribution, as well as physically compliant realizations obtained from the QuaDRiGa model [37]. We treat the number of iterations  $J$  as a pre-defined requirement, and train our algorithm to minimize its loss within this number of iterations. The signal-to-noise ratio (SNR) is defined as  $1/\sigma_w^2$ .

We compare our unfolded optimizer ( $U$ -PGA+M) with the following benchmarks:

- **PGA + M**: running PGA with momentum (Algorithm 1) with fixed hyperparameters  $\{\mu, \beta\}, \forall j = 1 \dots J$ , chosen from a discrete grid, to maximize the average  $R$  after  $J = 500$  iterations for the entire training set.
- **Line Search**: PGA where the hyperparameters  $\{\mu_j, \beta_j\}_{j=0}^{J-1}$  are selected for each iteration through grid search to maximize the achievable rate  $R$  at each step [40]. This method performs an exhaustive search to find the optimal step size for each iteration, independently for each data sample, at the cost of excessive additional processing latency.
- **Manifold Optimization (MO)**: The optimizer proposed in [23] for centralized architectures, adapted to support modular beamformers. It suggests a relaxed version of the maximization problem (7), taking gradient steps of  $\mathbf{W}$  toward the fully digital beamformer  $\mathbf{G}_{\text{opt}}$ , trying to minimize the error  $\|\mathbf{W}\mathbf{A} - \mathbf{G}_{\text{opt}}\|^2$ , and projecting the resulted matrix  $\mathbf{W}$  on the feasible set, using  $\mathcal{P}_{\mathcal{W}}(\cdot)$ . As in the *Line Search* benchmark, it performs an exhaustive line search to choose the best step size for each iteration.
- **CNN**: A CNN based on the architecture of [27], trained to map channel realizations  $\{\mathbf{H}[b]\}_{b=1}^B$  into the phases of  $\mathbf{W}$  that maximize the channel-rate  $R$ . This approach is extremely parameterized. For example, in a system with  $K = 7$  users,  $M = 8$  antennas, and  $B = 4$  frequency bins, the CNN consists of 274088 learned parameters, whereas  $U$ -PGA+M has only 960 parameters.

### B. Unconstrained Modular Beamformers

We start the experimental study by considering unconstrained modular beamformers, as described in Subsection **III-B**. Our evaluation first focuses on small scale MIMO settings, after which we assess transferability to larger systems.

1) **Small-Scale Hybrid Modular MIMO**: We first examine two scenarios representing relatively small-scale settings. In **Scenario 1**, we set  $(T = 5, P = 2, L = 4, N = 20, B = 2, K = 20)$ , and the channel matrices obey Rayleigh fading. **Scenario 2** uses QuaDRiGa channels with  $(T = 5, P = 4, L = 2, N = 3, B = 4, K = 5)$ .

We use these scenarios to evaluate the ability of our unfolded design to improve the sum-rate achieved within  $J = 10$  iterations. To that aim, we depict in Figs. 5-6 the average sum-rate vs. the iteration index  $j$  for **Scenarios 1** and **2**, respectively. For fair comparison, we set all optimization-

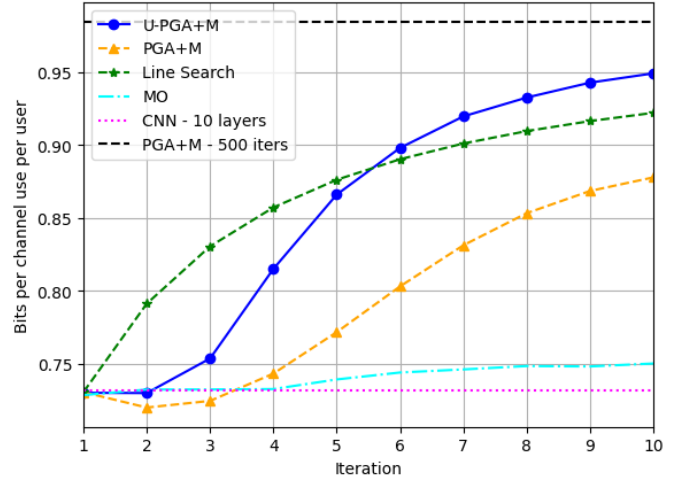


Fig. 5: Sum-rate vs. iteration, **Scenario 1**, SNR = 0 dB.

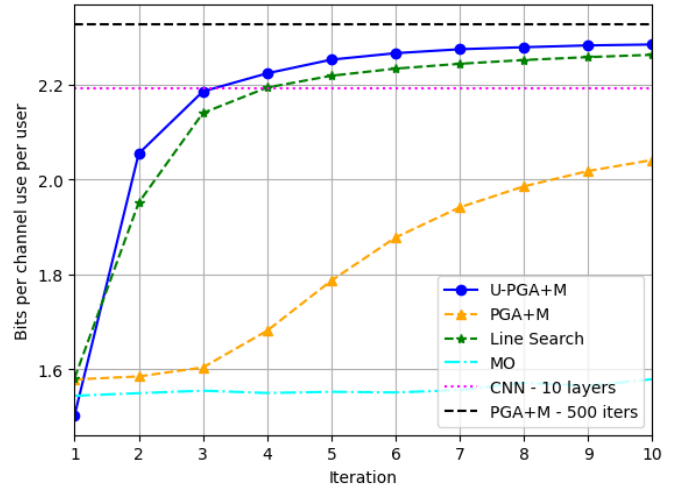


Fig. 6: Sum-rate vs. iteration, **Scenario 2**, SNR = 0 dB.

based algorithms to have  $J = 10$  iterations, with the *CNN* having 10 layers, and compare the sum-rate to that achieved by *PGA+M* with  $J = 500$  iterations. We consistently observe that in the considered scenarios with a limited number of iterations, our unfolded PGA outperforms all benchmarks, including the costly and greedy line search hyperparameter setting, and the highly parameterized CNN benchmark. The latter particularly struggles in Rayleigh channels, as CNNs tends to capture spatial relationships, and such relationships do not exist under Rayleigh fading. Similarly, the MO optimizer exhibits slow convergence due to the additional modular structure imposed in our setting of modular beamformers.

The results after  $J$  iterations illustrated in Figs. 5-6 are also reported in Table I, along with latency of the various methods. The latter is evaluated for all algorithms on the same platform (Google Colab premium). We notice in Table I that the unfolded algorithm is 30 – 50 times faster than optimizers that employ line search or run a large number of iterations, while achieving a comparable sum-rate. The *CNN* benchmark has the least latency here, owing to the efficient implementation and natural support of such architectures in platforms such as Google Colab. This efficiency persists across multiple scenarios, emphasizing our ability to provide reliable

Algorithm	$J$	Scenario 1	Scenario 2	Scenario 3	Latency[ $\mu$ s]
U-PGA+M	10	0.95	2.28	0.414	417
PGA+M	10	0.88	2.04	0.407	413
	500	0.98	2.33	0.421	19352
Line Search	10	0.92	2.26	0.415	123705
CNN	10	0.73	2.19	0.388	290
MO	10	0.75	1.58	0.388	31767

TABLE I: Sum-rate and running time for different **Scenarios 1, 2, and 3**. In **Scenario 3**, *U-PGA+M* was originally trained on **Scenario 4**. *Latency* relates to the computation time of a single channel realization in **Scenario 2**.

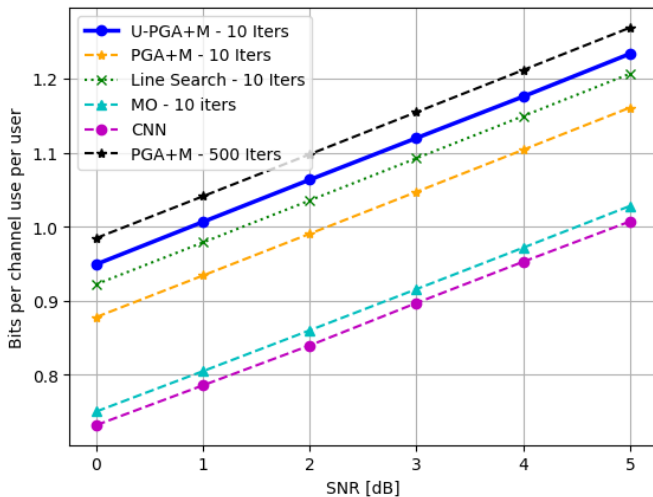


Fig. 7: Sum-rate vs. SNR, **Scenario 1**.

modular beamformers with minimal latency, that can be further enhanced by employing dedicated hardware accelerators.

Figs. 7 and 8 show the resulted sum-rate for each benchmark in a wide range of SNR values, for **Scenarios 1 and 2**, respectively. There, we observe that the gains obtained by the unfolded algorithm while using the same number of iterations, are translated into SNR gains of 1.25 – 1.5 dB compared to the *PGA + M* algorithm with the same  $J$  iterations.

### 2) Transferable Modular Structures Simulation Results:

As explained in Subsection III-B3, one of the key advantages of our learn-to-optimize modular beamforming design is the

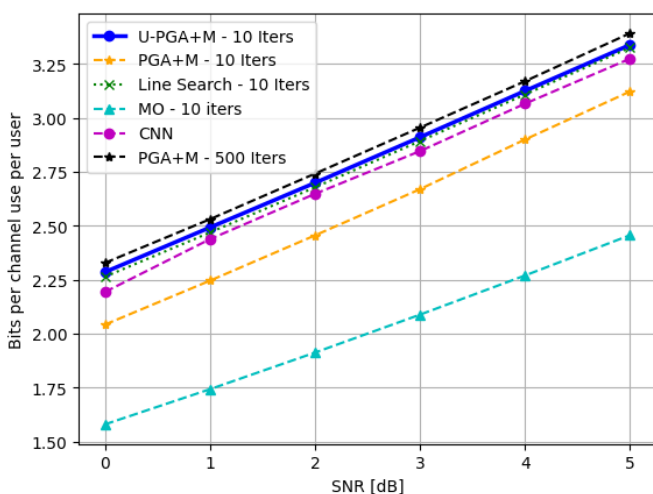


Fig. 8: Sum-rate vs. SNR, **Scenario 2**.

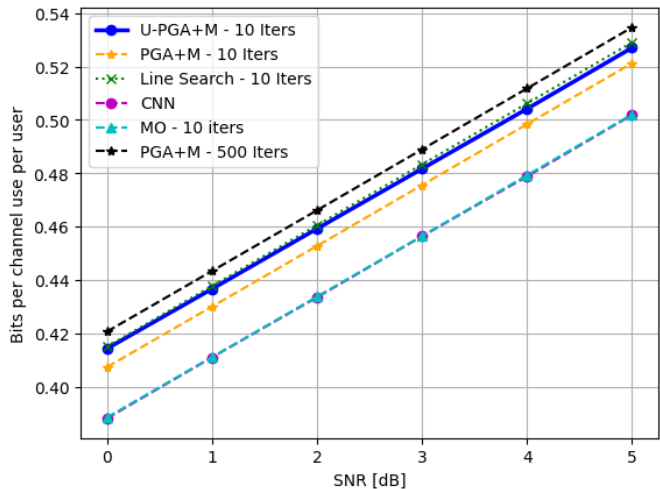


Fig. 9: Sum-rate vs. SNR, **Scenario 4** ( $K = 50$  users). Here, *U-PGA+M* was trained on  $K = 5$  users.

transferability of learned parameters when scaling the system. Modular structures allow us to train the system with specific settings and then scale it up to a larger number of users or panels without needing to retrain the model.

**Scaling the number of users:** To demonstrate this, we first evaluate *U-PGA+M* that was initially trained with a small number of users,  $K = 5$ , and then deployed in a system with a large number of users,  $K = 50$ , using the same hyperparameters. This example illustrates the transferability of the unfolded model. For this evaluation, we introduce **Scenario 3**: ( $T = 5, P = 8, N = 4, B = 2, K = 50$ ) and **Scenario 4**: ( $T = 5, P = 8, N = 4, B = 2, K = 5$ ). In both scenarios the channel realizations are sampled from a Rayleigh fading distribution. Fig. 9, presents the sum-rates achieved by the various benchmarks on **Scenario 3**, along with the performance of the *U-PGA+M* algorithm, which was trained on **Scenario 4**. These results demonstrate the flexibility of the unfolded algorithm and underscore its advantages in adapting to rapidly changing environments. The average rates at SNR of 0 are also reported in Table I.

**Scaling the number of panels:** Next, we provide an example of scaling up the number of panels. In this example, we use  $c = 8$  as the scaling coefficient, and increase the number of panels from  $P$  to  $c \cdot P$ , using  $\{\alpha_j, \beta_j\} = \{I_c \otimes \alpha_j, I_c \otimes \beta_j\}$ . To this end, we introduce **Scenario 5**: ( $T = 5, P = 2, N = 4, B = 2, K = 7$ ) and **Scenario 6**: ( $T = 5 \cdot 8, P = 2 \cdot 8, N = 4, B = 2, K = 7$ ); both obey Rayleigh fading. Fig. 10 illustrates the results of various benchmarks trained on **Scenario 6**, alongside the performance of the *U-PGA+M* algorithm that was trained on **Scenario 5**. These results highlight the flexibility of our design, demonstrating how it can be initially trained on a smaller network, perform straightforward calculations, and then be effectively scaled to much larger and more complex systems.

### C. Power-Aware Modular Beamformers

We proceed to evaluating the ability of our unfolded optimizer to encourage power-efficient modular beamformers. We

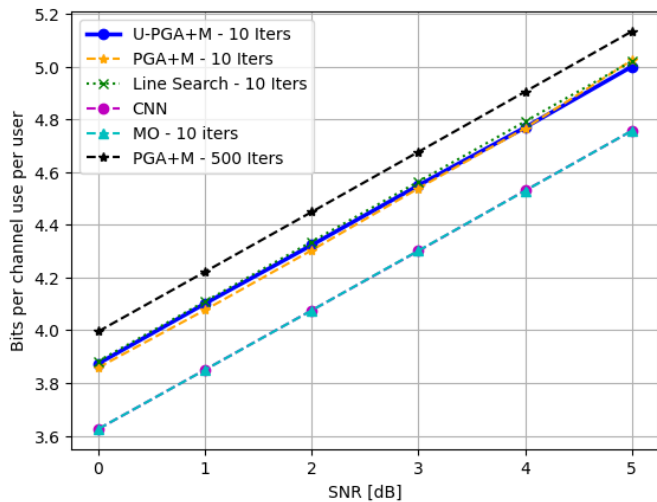


Fig. 10: Sum-rate vs. SNR, **Scenario 6**. Here,  $U$ -PGA+M was trained on  $M = 8$ , and deployed on  $M = 64$ .

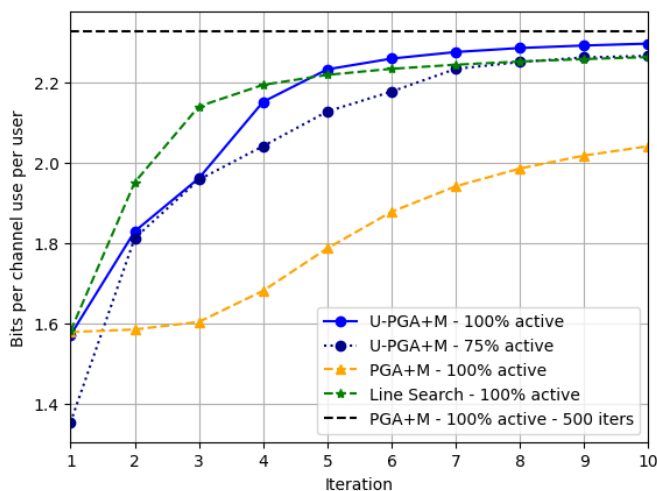


Fig. 11: Sum-rate vs. iteration, **Scenario 2**, SNR = 0 dB.

divide our evaluation to boosting efficiency via deactivating phase shifters, and via using low resolution phase shifters.

1) *Sparse Modular Beamformers*: We evaluate the effect of designing modular beamformers with deactivated phase shifters by boosting sparsity in  $\mathbf{W}$ . We focus on **Scenario 2**, and apply  $U$ -PGA+M using Algorithm 3 utilizing the projection step  $\mathcal{P}_{\mathcal{W}}(\cdot)$  in (18). We set the parameter  $S_{\max}$  to be  $0.75 \cdot N \cdot L \cdot P$ . As the benchmarks detailed in Subsection V-A do not naturally account for such constraints, we compare here  $U$ -PGA+M to unconstrained settings that are based on PGA, possibly with line search and/or large number of iterations.

The resulting rates vs. iteration compared to those achieved without such power-aware design are reported in Fig. 11. We observe that by applying Algorithm 3, one achieves a 25% reduction in active components while maintaining a comparable sum-rate and identical running time to unconstrained settings. The unfolded algorithm learns to rapidly compensate for the inactive components by tuning the active phase shifters. Fig. 12 further highlights the advantages of the unfolded power-aware algorithm by evaluating the resulting sum-rate over different SNRs. There, we observe that our power-aware

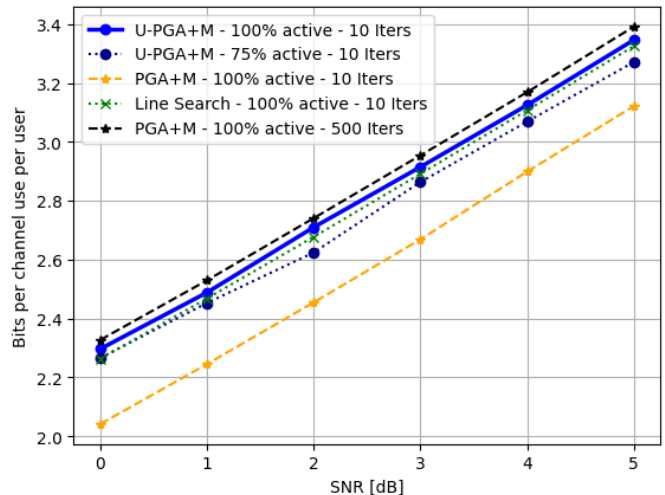


Fig. 12: Sum-rate vs. SNR, **Scenario 2**

design not only allows accurate operation with 25% of the phase shifters deactivated, but it also offers approximately 1 dB improvement in SNR over the  $PGA + M$  benchmark with the same number of iterations.

2) *Low-Resolution Modular Beamformers*: We conclude our numerical study by evaluating the effect of using quantized phase shifters, and the ability of our power-aware design to account for such constraint when tuning modular beamformers. We consider the power-aware Algorithm 3, utilizing the projection step for  $\mathcal{P}_{\mathcal{W}}(\cdot)$  as specified in (20), when the phase shifters can be configured to merely 4 bits in phase, i.e.,  $Q = 16$ . The benchmarks detailed in Subsection V-A are adapted to produce low-resolution phase shifters by altering the projection step (for optimization methods) or quantizing the produced phases (for the CNN).

The resulting sum-rate vs. iteration and vs. SNR for **Scenario 1** are illustrated in Figs. 13 and 14, respectively. The results demonstrate that the proposed unfolded algorithm, which is particularly geared to accounting for low-resolution phase shifters, significantly outperforms other benchmarks, including both slow iterative methods that are not trained as machine learning models, and suffer more notable degradation due to quantization, as well as the heavily parameterized CNN. Specifically, while  $PGA + M$  struggles to overcome the quantization constraints using gradient steps, and tends to converge to a local maximum, the unfolded algorithm effectively learns to traverse the loss surface and projection constraints, achieving a better sum-rate. As shown in Fig. 14, the unfolded algorithm consistently performs better across various SNR values compared to all other benchmarks.

## VI. CONCLUSIONS

In this work, we investigated rapid beamforming design for uplink modular MIMO systems under three different sets of constraints: unconstrained phase shifters, sparse phase shifters, and quantized phase shifters. Our proposed algorithm, a momentum-aided gradient-based optimization of the sum-rate objective, boosts power efficient settings while operating with a fixed and small number of iterations. By transforming the optimizer into a lightweight, trainable model, we

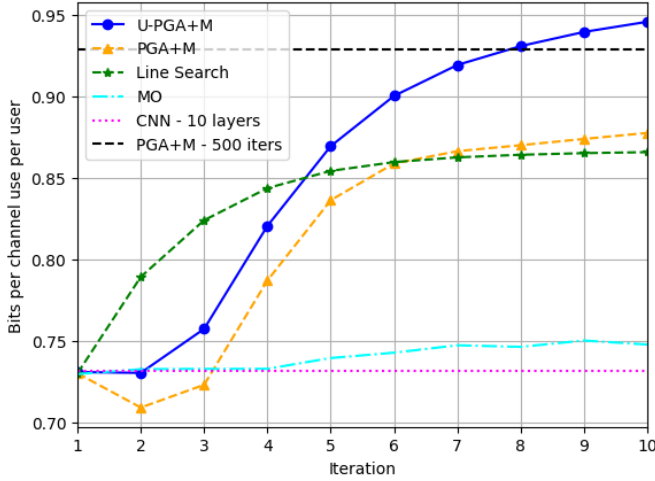


Fig. 13: Sum-rate vs. iteration, **Scenario 1**, 4-bit phase shifters, SNR = 0 dB.

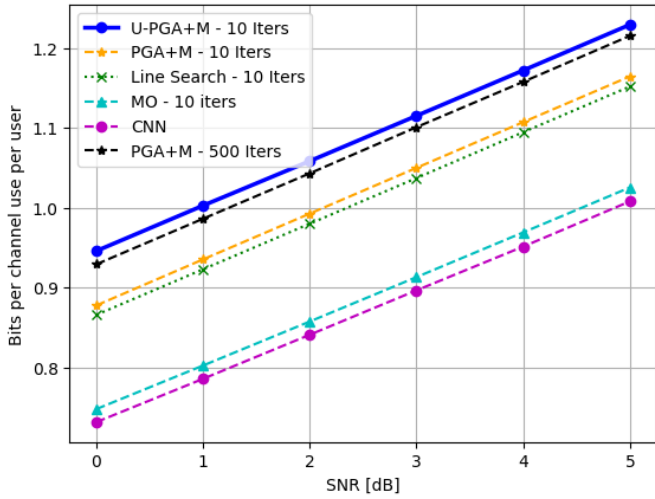


Fig. 14: Sum-rate vs. SNR, **Scenario 1**, 4-bit phase shifters.

harness data to fine-tune its hyperparameters, enhancing its adaptability to various system conditions. Our experimental results demonstrate a significant improvement in the achieved sum-rate compared to benchmarks operating within the same computational-time constraints, while also surpassing other benchmarks in hardware-aware and power-aware designs.

## APPENDIX

### A. Proof of Theorem 1

For ease of presentation, we define the following auxiliary variables:  $\mathbf{G}^\dagger \triangleq (\mathbf{G}^H \mathbf{G})^{-1} \mathbf{G}^H$ ,  $\mathbf{P} \triangleq \mathbf{G} \mathbf{G}^\dagger$ ,  $\mathbf{Z}[b] \triangleq \mathbf{P} \mathbf{H}[b] \mathbf{H}^H [b]$ , and  $\mathbf{Q}[b] \triangleq \mathbf{I}_k + \frac{\rho_s}{\sigma_w^2} \mathbf{Z}[b]$ . Using these symbols, the objective with respect to which the derivative is taken can be written as  $R(\mathbf{G}; \{\mathbf{H}[b]\}) = \frac{1}{B} \sum_{b=1}^B \log |\mathbf{Q}[b]|$ . Plugging-in auxiliary variables, we aim at proving Theorem 1 by showing that

$$\nabla_{\mathbf{W}} R(\mathbf{W}, \mathbf{A}) = \frac{1}{B} \sum_{b=1}^B \left( \frac{\rho_s}{\sigma_w^2} \mathbf{A} \mathbf{G}^\dagger \mathbf{H}[b] \mathbf{H}[b]^H \mathbf{Q}^{-1} (\mathbf{I} - \mathbf{P}) \right)^H. \quad (\text{A.1})$$

The representation in (A.1) can be derived using the differential method for matrices as described in [50]. In the following proof the sign  $\cdot$  denotes the Frobenius inner product, and the derivations are done using chain rule. For brevity we include our derivation for a single frequency bin.

Since  $R = \log |\mathbf{Q}|$  when  $B = 1$ , it holds that the differential can be expressed as

$$\begin{aligned} dR &= \left( \mathbf{Q}^{-1} \right)^H : d\mathbf{Q} \stackrel{(a)}{=} \left( \mathbf{Q}^{-1} \right)^H : \frac{\rho_s}{\sigma_w^2} d\mathbf{Z} \\ &\stackrel{(b)}{=} \left( \frac{\rho_s}{\sigma_w^2} \mathbf{Q}^{-1} \right)^H : d\mathbf{Z} \stackrel{(c)}{=} \left( \frac{\rho_s}{\sigma_w^2} \mathbf{Q}^{-1} \right)^H : d\mathbf{P} \mathbf{H} \mathbf{H}^H \\ &\stackrel{(d)}{=} \left( \frac{\rho_s}{\sigma_w^2} \mathbf{H} \mathbf{H}^H \mathbf{Q}^{-1} \right)^H : (\mathbf{I} - \mathbf{P}) d\mathbf{G} \mathbf{G}^\dagger \end{aligned} \quad (\text{A.2})$$

where (a) stems from  $d\mathbf{Q} = d\mathbf{I}_k + d\frac{\rho_s}{\sigma_w^2} \mathbf{Z} = \frac{\rho_s}{\sigma_w^2} d\mathbf{Z}$ , (b) and (d) are based on the Hermitian property inner product, and (c) stems from  $d\mathbf{Z} = d\mathbf{P} \mathbf{H} \mathbf{H}^H$ , as  $\mathbf{H}$  is independent of  $\mathbf{W}$ .

Next, we substitute  $\mathbf{P}$ ,  $\mathbf{G}^\dagger$ , and  $\mathbf{G}$  using chain rule:

$$dR = \left( \frac{\rho_s}{\sigma_w^2} (\mathbf{H} \mathbf{H}^H \mathbf{Q}^{-1}) \right)^H : (\mathbf{I} - \mathbf{P}) d\mathbf{G} \mathbf{G}^\dagger. \quad (\text{A.3})$$

Equation (A.3) can be explained by recalling that  $\mathbf{P} \triangleq \mathbf{G} (\mathbf{G}^H \mathbf{G})^{-1} \mathbf{G}^H$ , and thus

$$\begin{aligned} d\mathbf{P} &= d\mathbf{G} (\mathbf{G}^H \mathbf{G})^{-1} \mathbf{G}^H + \mathbf{G} d(\mathbf{G}^H \mathbf{G})^{-1} \mathbf{G}^H \\ &\quad + \mathbf{G} (\mathbf{G}^H \mathbf{G})^{-1} d\mathbf{G}^H \\ &= d\mathbf{G} \mathbf{G}^\dagger - \mathbf{G} (\mathbf{G}^H \mathbf{G})^{-1} (d\mathbf{G}^H \mathbf{G} + \mathbf{G}^H d\mathbf{G}) \mathbf{G}^\dagger \\ &= d\mathbf{G} \mathbf{G}^\dagger - \mathbf{G} (\mathbf{G}^H \mathbf{G})^{-1} \mathbf{G}^H d\mathbf{G} \mathbf{G}^\dagger \\ &= (\mathbf{I} - \mathbf{P}) d\mathbf{G} \mathbf{G}^\dagger. \end{aligned}$$

In (A.4), the term  $d\mathbf{G}^H$  vanishes since  $\mathbf{G}^H$  is independent of  $\mathbf{G}$ , and thus independent of  $\mathbf{W}$ . Once (A.3) is achieved, the rest of the proof becomes straight forward, using the chain rule until (A.1) is reached, i.e.,

$$\begin{aligned} dR &= \left( \frac{\rho_s}{\sigma_w^2} \mathbf{G}^\dagger \mathbf{H} \mathbf{H}^H \mathbf{Q}^{-1} (\mathbf{I} - \mathbf{P}) \right)^H : d\mathbf{G} \\ &= \left( \frac{\rho_s}{\sigma_w^2} \mathbf{G}^\dagger \mathbf{H} \mathbf{H}^H \mathbf{Q}^{-1} (\mathbf{I} - \mathbf{P}) \right)^H : d\mathbf{W} \mathbf{A} \\ &= \left( \frac{\rho_s}{\sigma_w^2} \mathbf{A} \mathbf{G}^\dagger \mathbf{H} \mathbf{H}^H \mathbf{Q}^{-1} (\mathbf{I} - \mathbf{P}) \right)^H : d\mathbf{W}, \end{aligned} \quad (\text{A.4})$$

which concludes that  $\nabla_{\mathbf{W}} R(\mathbf{W}, \mathbf{A}) = \left( \frac{\rho_s}{\sigma_w^2} \mathbf{A} \mathbf{G}^\dagger \mathbf{H} \mathbf{H}^H \mathbf{Q}^{-1} (\mathbf{I} - \mathbf{P}) \right)^H$ , thus proving the theorem.

## REFERENCES

- [1] O. Levy and N. Shlezinger, "Rapid hybrid modular receive beamforming via learned optimization," in *IEEE International Conference on Acoustics, Speech and Signal Processing (ICASSP)*, 2024, pp. 12 826–12 830.
- [2] Z. Wang, J. Zhang, H. Du, D. Niyato, S. Cui, B. Ai, M. Debbah, K. B. Letaief, and H. V. Poor, "A tutorial on extremely large-scale MIMO for 6G: Fundamentals, signal processing, and applications," *IEEE Commun. Surveys Tuts.*, 2024.
- [3] E. Björnson, C.-B. Chae, R. W. Heath Jr, T. L. Marzetta, A. Mezghani, L. Sanguinetti, F. Rusek, M. R. Castellanos, D. Jun, and Ö. T. Demir, "Towards 6G MIMO: Massive spatial multiplexing, dense arrays, and interplay between electromagnetics and processing," *arXiv preprint arXiv:2401.02844*, 2024.

- [4] E. Björnson, L. Sanguinetti, H. Wymeersch, J. Hoydis, and T. L. Marzetta, "Massive MIMO is a reality—what is next?: Five promising research directions for antenna arrays," *Digital Signal Processing*, vol. 94, pp. 3–20, 2019.
- [5] E. Björnson and L. Sanguinetti, "Scalable cell-free massive MIMO systems," *IEEE Trans. Commun.*, vol. 68, no. 7, pp. 4247–4261, 2020.
- [6] S. Malkowsky *et al.*, "The world's first real-time testbed for massive MIMO: Design, implementation, and validation," *IEEE Access*, vol. 5, pp. 9073–9088, 2017.
- [7] O. L. López, D. Kumar, R. D. Souza, P. Popovski, A. Tölli, and M. Latva-Aho, "Massive MIMO with radio stripes for indoor wireless energy transfer," *IEEE Trans. Wireless Commun.*, vol. 21, no. 9, pp. 7088–7104, 2022.
- [8] T. Raviv, S. Park, O. Simeone, Y. C. Eldar, and N. Shlezinger, "Adaptive and flexible model-based AI for deep receivers in dynamic channels," *IEEE Wireless Commun.*, 2024.
- [9] A. F. Molisch, V. V. Ratnam, S. Han, Z. Li, S. L. H. Nguyen, L. Li, and K. Haneda, "Hybrid beamforming for massive MIMO: A survey," *IEEE Commun. Mag.*, vol. 55, no. 9, pp. 134–141, 2017.
- [10] R. Méndez-Rial, C. Rusu, N. González-Prelcic, A. Alkhateeb, and R. W. Heath, "Hybrid MIMO architectures for millimeter wave communications: Phase shifters or switches?" *IEEE Access*, vol. 4, pp. 247–267, 2016.
- [11] S. S. Ioushua and Y. C. Eldar, "A family of hybrid analog–digital beamforming methods for massive MIMO systems," *IEEE Trans. Signal Process.*, vol. 67, no. 12, pp. 3243–3257, 2019.
- [12] T. Gong, N. Shlezinger, S. S. Ioushua, M. Namer, Z. Yang, and Y. C. Eldar, "RF chain reduction for MIMO systems: A hardware prototype," *IEEE Syst. J.*, vol. 14, no. 4, pp. 5296–5307, 2020.
- [13] S. Park, A. Alkhateeb, and R. W. Heath, "Dynamic subarrays for hybrid precoding in wideband mmWave MIMO systems," *IEEE Trans. Wireless Commun.*, vol. 16, no. 5, pp. 2907–2920, 2017.
- [14] R. Li, H. Yan, and D. Cabric, "Rainbow-link: Beam-alignment-free and grant-free mmW multiple access using true-time-delay array," *IEEE J. Sel. Areas Commun.*, vol. 40, no. 5, pp. 1692–1705, 2022.
- [15] E. Tasci, T. Zirtiloglu, A. Yasar, Y. C. Eldar, N. Shlezinger, and R. T. Yazicigil, "Robust task-specific beamforming with low-resolution ADCs for power-efficient hybrid MIMO receivers," *arXiv preprint arXiv:2212.00107*, 2022.
- [16] N. Shlezinger, G. C. Alexandropoulos, M. F. Imani, Y. C. Eldar, and D. R. Smith, "Dynamic metasurface antennas for 6G extreme massive MIMO communications," *IEEE Wireless Commun.*, vol. 28, no. 2, pp. 106–113, 2021.
- [17] Y. Gabay, N. Shlezinger, T. Routtenberg, Y. Ghasempour, G. C. Alexandropoulos, and Y. C. Eldar, "Leaky waveguide antennas for downlink wideband THz communications," in *IEEE International Conference on Acoustics, Speech and Signal Processing (ICASSP)*, 2024, pp. 9111–9115.
- [18] A. M. Elbir, K. V. Mishra, S. A. Vorobyov, and R. W. Heath Jr, "Twenty-five years of advances in beamforming: From convex and nonconvex optimization to learning techniques," *IEEE Signal Process. Mag.*, vol. 40, no. 4, pp. 118–131, 2023.
- [19] N. Shlezinger, M. Ma, O. Lavi, N. T. Nguyen, Y. C. Eldar, and M. Juntti, "AI-empowered hybrid MIMO beamforming," *IEEE Veh. Technol. Mag.*, 2024.
- [20] X. Yu, J.-C. Shen, J. Zhang, and K. B. Letaief, "Alternating minimization algorithms for hybrid precoding in millimeter wave MIMO systems," *IEEE J. Sel. Topics Signal Process.*, vol. 10, no. 3, pp. 485–500, 2016.
- [21] F. Sohrabi and W. Yu, "Hybrid digital and analog beamforming design for large-scale antenna arrays," *IEEE J. Sel. Topics Signal Process.*, vol. 10, no. 3, 2016.
- [22] X. Qiao, Y. Zhang, M. Zhou, and L. Yang, "Alternating optimization based hybrid precoding strategies for millimeter wave MIMO systems," *IEEE Access*, vol. 8, pp. 113 078–113 089, 2020.
- [23] X. Yu, J.-C. Shen, J. Zhang, and K. B. Letaief, "Alternating minimization algorithms for hybrid precoding in millimeter wave mimo systems," *IEEE Journal of Selected Topics in Signal Processing*, vol. 10, no. 3, pp. 485–500, 2016.
- [24] A. Zappone, M. Di Renzo, and M. Debbah, "Wireless networks design in the era of deep learning: Model-based, AI-based, or both?" *IEEE Trans. Commun.*, vol. 67, no. 10, pp. 7331–7376, 2019.
- [25] T. Chen, X. Chen, W. Chen, H. Heaton, J. Liu, Z. Wang, and W. Yin, "Learning to optimize: A primer and a benchmark," *The Journal of Machine Learning Research*, vol. 23, no. 1, pp. 8562–8620, 2022.
- [26] A. M. Elbir and A. K. Papazafeiropoulos, "Hybrid precoding for multiuser millimeter wave massive MIMO systems: A deep learning approach," *IEEE Trans. Veh. Technol.*, vol. 69, no. 1, pp. 552–563, 2019.
- [27] P. Dong, H. Zhang, and G. Y. Li, "Framework on deep learning-based joint hybrid processing for mmWave massive MIMO systems," *IEEE Access*, vol. 8, pp. 106 023–106 035, 2020.
- [28] O. Lavi and N. Shlezinger, "Learn to rapidly and robustly optimize hybrid precoding," *IEEE Trans. Commun.*, vol. 71, no. 10, pp. 5814–5830, 2023.
- [29] N. T. Nguyen, M. Ma, N. Shlezinger, Y. C. Eldar, A. Swindlehurst, and M. Juntti, "Deep unfolding hybrid beamforming designs for THz massive MIMO systems," *IEEE Trans. Signal Process.*, vol. 71, pp. 3788–3804, 2023.
- [30] E. Balevi and J. G. Andrews, "Unfolded hybrid beamforming with GAN compressed ultra-low feedback overhead," *IEEE Trans. Wireless Commun.*, vol. 20, no. 12, pp. 8381–8392, 2021.
- [31] S. Shi, Y. Cai, Q. Hu, B. Champagne, and L. Hanzo, "Deep-unfolding neural-network aided hybrid beamforming based on symbol-error probability minimization," *IEEE Trans. Veh. Technol.*, vol. 72, no. 1, pp. 529–545, 2022.
- [32] —, "Deep-unfolding neural-network aided hybrid beamforming based on symbol-error probability minimization," *IEEE Transactions on Vehicular Technology*, vol. 72, no. 1, pp. 529–545, 2023.
- [33] N. Shlezinger, Y. C. Eldar, and S. P. Boyd, "Model-based deep learning: On the intersection of deep learning and optimization," *IEEE Access*, vol. 10, pp. 115 384–115 398, 2022.
- [34] J. V. Alegría, F. Rusek, and O. Edfors, "Trade-offs in decentralized multi-antenna architectures: The WAX decomposition," *IEEE Trans. Signal Process.*, vol. 69, pp. 3627–3641, 2021.
- [35] J. V. Alegría and F. Rusek, "Trade-offs in decentralized multi-antenna architectures: Sparse combining modules for WAX decomposition," *IEEE Trans. Signal Process.*, vol. 71, pp. 2879–2894, 2023.
- [36] N. Shlezinger, J. Whang, Y. C. Eldar, and A. G. Dimakis, "Model-based deep learning," *Proc. IEEE*, vol. 111, no. 5, pp. 465–499, 2023.
- [37] S. Jaeckel, L. Raschkowski, K. Börner, and L. Thiele, "QuADRIGa: A 3-D multi-cell channel model with time evolution for enabling virtual field trials," *IEEE Trans. Antennas Propag.*, vol. 62, no. 6, pp. 3242–3256, 2014.
- [38] J. Deng, O. Tirkkonen, and C. Studer, "MmWave multiuser MIMO precoding with fixed subarrays and quantized phase shifters," *IEEE Trans. Veh. Technol.*, vol. 68, no. 11, pp. 11 132–11 145, 2019.
- [39] N. Shlezinger, O. Dicker, Y. C. Eldar, I. Yoo, M. F. Imani, and D. R. Smith, "Dynamic metasurface antennas for uplink massive MIMO systems," *IEEE Trans. Commun.*, vol. 67, no. 10, pp. 6829–6843, 2019.
- [40] S. P. Boyd and L. Vandenberghe, *Convex optimization*. Cambridge university press, 2004.
- [41] N. Shlezinger and T. Routtenberg, "Discriminative and generative learning for linear estimation of random signals [lecture notes]," *IEEE Signal Process. Mag.*, vol. 40, no. 6, pp. 75–82, 2023.
- [42] N. Samuel, T. Diskin, and A. Wiesel, "Learning to detect," *IEEE Trans. Signal Process.*, vol. 67, no. 10, pp. 2554–2564, 2019.
- [43] T. Alter and N. Shlezinger, "Rapid optimization of superposition codes for multi-hop NOMA MANETs via deep unfolding," *arXiv preprint arXiv:2406.05747*, 2024.
- [44] Y. Noah and N. Shlezinger, "Limited communications distributed optimization via deep unfolded distributed ADMM," *arXiv preprint arXiv:2309.14353*, 2023.
- [45] V. V. Ratnam, J. Mo, A. Alammouri, B. L. Ng, J. Zhang, and A. F. Molisch, "Joint phase-time arrays: A paradigm for frequency-dependent analog beamforming in 6G," *IEEE Access*, vol. 10, pp. 73 364–73 377, 2022.
- [46] Y. C. Eldar and G. Kutyniok, *Compressed sensing: theory and applications*. Cambridge University Press, 2012.
- [47] E. Agustsson, F. Mentzer, M. Tschannen, L. Cavigelli, R. Timofte, L. Benini, and L. V. Gool, "Soft-to-hard vector quantization for end-to-end learning compressible representations," *Advances in neural information processing systems*, vol. 30, 2017.
- [48] N. Shlezinger, A. Amar, B. Luitjen, R. J. Van Sloun, and Y. C. Eldar, "Deep task-based analog-to-digital conversion," *IEEE Trans. Signal Process.*, vol. 70, pp. 6021–6034, 2022.
- [49] N. Lang, I. Assaf, O. Bokobza, and N. Shlezinger, "Data-driven lattices for vector quantization," in *IEEE International Conference on Acoustics, Speech and Signal Processing (ICASSP)*, 2024, pp. 8080–8084.
- [50] J. R. Magnus and H. Neudecker, *Matrix Differential Calculus with Applications in Statistics and Econometrics*, 2nd ed. John Wiley, 1999.